CHEIA TRACKING RADAR,

MEASUREMENT RESULTS AND LESSONS LEARNED

Liviu Ionescu(1), Roberto Scagnoli(1), Calin Bira(2), Radu Hobincu(2), Daniel Bostan(1)

(1)RARTEL S.A., 011041 Bucharest, Romania, liviu.ionescu@rartel.ro
(2) Faculty of Electronics, Telecommunications and Information Technology, Politehnica University of Bucharest, 060042 Bucharest, Romania

ABSTRACT

The constantly increasing number of space objects and debris orbiting Earth generate high risks for satellites and space vehicles, both in orbit and during the launching process. Furthermore, the re-entering objects create potential threat to people and assets on the ground. The European Space Policy for the 2021-2027 period, acknowledges the need for risk evaluation and collision avoidance, including a dedicated chapter for Space Situational Awareness (SSA) and requires the establishment of a Framework for Space Surveillance and Tracking (EUSST) Support. As part of this effort, a new space tracking sensor, the CHEIA_RO tracking radar, has been developed, implemented and commissioned in Romania, under the ESA SSA P3-SST-V - CHEIA PHASE 2 contract, by Rartel SA. The main purpose of the radar consists in tracking LEO objects but, in limited cases, tracking re-entry objects can be achieved. The radar was developed as a Linear Frequency Modulated Continuous Wave (LFMCW), software defined radar by reusing two decommissioned 32m Intelsat communication antennas placed in a difficult electromagnetic environment. Besides the environment, the 45 years old antennas came with limitations of their own. To overcome the challenges, the radar processes the return signal completely in the frequency domain. The present paper gives an overview of the final implementation architecture and presents and discusses the radar calibration measurements results. The measured Range, Doppler and angular data is compared to the initial TLE data and to the post factum high precision published orbital data that was obtained through optical means. Special chapters are dedicated to the challenges and to the lessons learned during implementation.

Keywords: Space Situational Awareness, Space Surveillance and Tracking, Cheia Radar, LFMCW Space Radar

INTRODUCTION

Romania, represented by the Romanian Space Agency (ROSA), is a member of the EU SST consortium and has a significant contribution to the European SST system. ROSA operates the national SST Operational Centre that coordinates the contribution of the Romanian sensors within the consortium. The sensor network currently includes several optical telescopes that have already provided timely and valuable data to the EU SST. ROSA has coordinated and participated in efforts to add a Romanian radar sensor to the consortium's assets [1].

The choice of adding a tracking radar sensor to the Romanian network for SST took into consideration its ability to operate in almost all weather conditions, day and night, without sensitivity to atmospheric or light pollution. The data provided by a tracking radar include several target's positions in polar coordinates (range and angles), as well as its radial velocity for a certain segment of its trajectory, in order to improve the estimation of its trajectory. As the majority of space debris around Earth is present in the LEO, this domain represents the priority interest for SST data collection activity. For this reason, the Romanian tracking radar sensor was designed track of targets within the LEO domain, i.e., 200–2000 km.

The task of developing a Romanian tracking radar sensor for SST applications was carried out by a consortium led by the local company RARTEL, a Romanian–Italian joint venture specialized in satellite services and applications. The preliminary study "SSA for Romania", funded by ESA, presented an inventory of existing facilities and infrastructure with associated technical know-how available at Romanian entities and capable to be integrated in international SSA, especially in SST activities. The survey also pointed to the possibility to develop the first Romanian radar sensor for SST data collection by reusing the 32m parabolic C-band antennas available at the National Satellite Communication Center in Cheia, Prahova County [11].

Proc. 9th European Conference on Space Debris, Bonn, Germany, 1–4 April 2025, published by the ESA Space Debris Office
Editors: S. Lemmens, T. Flohrer & F. Schmitz, (http://conference.sdo.esoc.esa.int, April 2025)

1. RADAR SITE OPPORTUNITIES AND CONSTRAINTS

The Cheia Satellite Communication Center in Prahova County, Romania, comprises two decommissioned 32 m diameter Cassegrain antennas originally installed in 1976 and 1979, respectively, positioned at latitude 45°27’24” N and longitude 25°56’48” E at a 900 m altitude. The antennas baseline is 80 m, and each antenna is mounted on top of its own support building.

The main reasons for the Cheia radar development at this site was the presence of the two high gain decommissioned antennas and the possibility to reuse them in a radar band. The advantage is of paramount budgetary importance since the cost of the antenna system represents an important portion of the total budget of any radar system.

The site is placed in a depression of a mountainous area, being surrounded by close and high mountains almost all around. Furthermore there are high firs close to the antennas. For the previous use as Intelsat communication, both conditions were acceptable but for the tracking radar use they posed serious challenges and restricted the minimum line of sight to 20° at all azimuths.

A supplemental advantage was provided by the existing infrastructure, consisting of dedicated buildings, waveguides connections between the antennas basements and the common data room and a redundant high power underground supply line.

To asses the suitability of the site for space radar, the estimation of the number of objects expected to pass through the antenna field of regard, and subsequently to be detectable by the radar was made using the ESA’s “PROOF-2009” software, as a basic simulation tool, and the subsequent post-processing was made using spreadsheet applications.

The histogram of the orbital regimes for the 20º minimum elevation limits and for all the passages is given in Figure 1[12].

The overall summary for the 20º minimum elevation limit case were:

- Number of satellites: 13725
- Number of passing: 47949

making the site disposition suitable for a tracking radar.

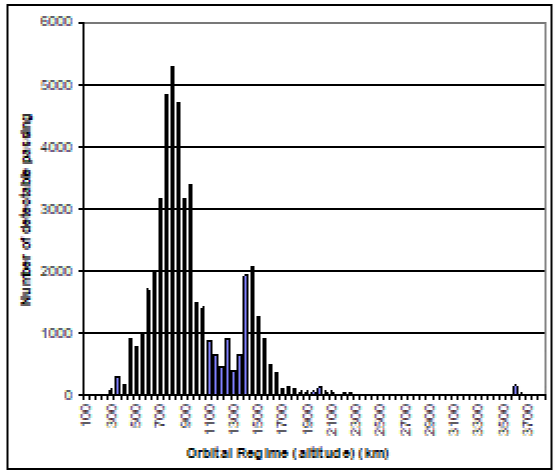

Figure 1 Histogram of the orbital regimes above 20º

The most important parameters of the antennas are presented in Table 1:

The electrical parameters of the antennas were measured in the feasibility study phase and confirmed during design and commissioning phases.

As can be seen, the two antennas have similar electrical parameters but different mechanical ones, making the implementation of autotracking on both antennas very difficult.

The antennas are very close (80m), Cheia 2 is partly masking Cheia 1 on the N direction at low elevations and a high communication tower is placed between the antennas as shown in Figure 2 [11]. This restricts further the tracking in some azimuth-elevation domain. As a supplemental disadvantage, the communication tower is full of microwave antennas and still holds C-band radio links, generating a crowded electromagnetic environment that affects the radar sensitivity and accuracy and requires special signal processing algorithms.

As can be seen from Table 1, even though decommissioned, the antennas were well conserved, with the antenna feeders in perfect state, that provided another significant budgetary advantage. However, this advantage came with the limitation of the transmitted power to 10 kW.

To take advantage of the antennas full capabilities including the antenna feeders and mitigate the low transmitted power limitation, the design of a Linear Frequency Modulation Continuous Wave (LFMCW) radar was almost compulsory. A design of a pulsed radar using very long pulses was also envisaged but the reliability constraints imposed by the available power amplifiers made the solution impossible to implement.

Table 1 Main technical specifications of the high gain antennas in Cheia Communications Center

Parameter	**Cheia 1**	**Cheia 2**
Model	Intelsat Std. A Earth Station Mark IV	Intelsat Std. A Earth Station Mark IVA
Manufacturer	Nippon Electric Co., Ltd. (NEC)	Nippon Electric Co., Ltd. (NEC)
Diameter	32 m	32 m
Year of installation	1976	1979
Originally used	Intelsat IS—905 at 335.5°E	Intelsat IS—904 at 60.0°E
Total weight	309 ton	260 ton
Azimuth scanning	-170°÷ +360° (vs. N) (after retrofit)	-170°÷ +360° (vs. N) (after retrofit)
Elevation scanning	0°–92°	0°–92°
Tracking speed	1°/s (after retrofit)	1°/s (after retrofit)
Tracking acceleration	$0.5°/s^2$ (after retrofit)	$0.5°/s^2$ (after retrofit)
Bandwidth	3.6–6.4 GHz	3.6–6.4 GHz
Antenna gain @6.0GHz	>63 dBi (@6.0GHz)	>63 dBi (@6.0GHz)
G/T factor (EL>20°)	>41	>41
Beamwidth	0.11°	0.11°
Polarization	Dual circular	Dual circular
Isolation between antennas	>93 dB	>93 dB
VSWR @6.0GHz (RH/LH port)	1,016/1.016	1,013/1.009
Maximum power @6.0GHz	10 kW	10 kW

Figure 2 Communication tower placed between the antennas

2. RADAR IMPLEMENTATION

The design of the new SST tracking radar was carried out based on the following hypotheses:

- Operation with two antennas in quasi-monostatic architecture with an 80 m baseline. In this setup, the Cheia 1 antenna would be used for transmitting (Tx) while the Cheia 2 antenna would be used for receiving (Rx) circular polarized wave. Both Cheia antennas positioning systems to be retrofitted.
- C-band radar. While the antenna bandwidth allowed operation in both S and C radar bands, in the C band, the antenna figure of merit is higher and the radar allocated frequency band is close and, partly overlapes the antenna C-band specified bandwidth of 5845–6425 MHz.
- Transmitted power below the antennas feders limit of 10 kW.

The radar was designed as a Continuous Wave (CW) radar, using Linear Frequency Modulation (LFM) of the transmitted signal. To preserve modulation linearity, a 5 kW SSPA power amplifier, operating at -3 dB from the 5 kW saturation point, was used. The SSPA power was chosen as an optimum value relative to the financial budget and the minimum size of detectable objects. The radar was designed with a software defined architecture, minimizing the number of analog blocks.

The radar was implemented as a common FMCW radar using mostly COTS as presented in Figure 3. To fit the design, some of the blocks had to be designed and produced in-house. This is the case of the Sum & Delta Receiver and of the Signal processor. They are based on COTS components but the design and implementation is in-house.

The low transmitted power had to be compensated through dedicated signal processing, completely designed and produced in-house. The particularity of the radar is that the target signal processing is performed completely in the frequency domain. This way of processing offers the minimum instantaneous frequency bandwidth, allowing the detection of small objects while relatively low transmitted power is used.

The antennas positioning systems were retrofitted to be capable of superior speed and acceleration performances compared to the original ones. The increased angular speed (1°/s as compared to the original 0.3°/s) and the increased angular acceleration (0.5°/s^2 as compared to the original 0.3°/s^2) were obtained by installing new drive motors and a modern antenna control system.

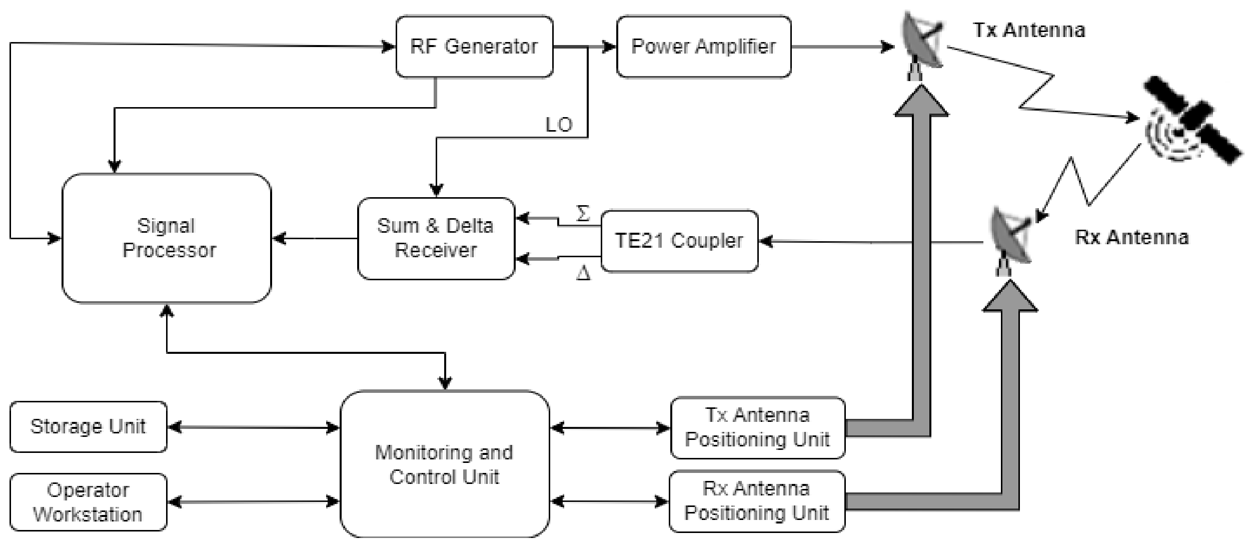

Figure 3 Cheia radar general diagram

The Monitoring and control Unit was implemented as a computational system that controls the radar operation through in-house designed and produced software algorithms and subsystems commands. It was implemented on a dedicated COTS server and its operation was designed to minimize the traffic between the radar's subsystems connected to the radar's LAN. The Monitoring and control Unit offers an user interface, as presented in Figure 4.

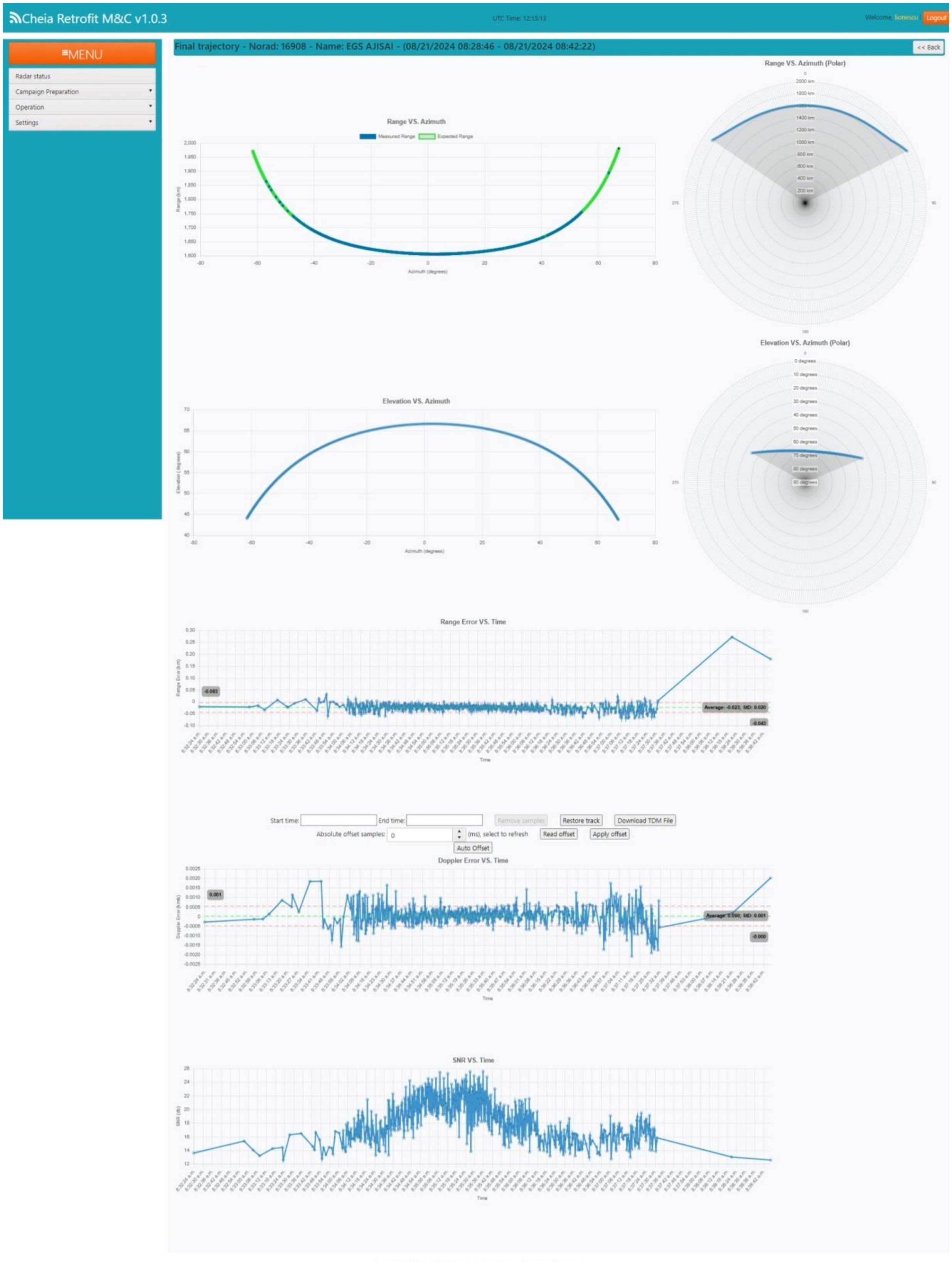

Figure 4 Radar user interface

The Monitoring and control Unit user interface displays:

- the measured Range-Azimuth target track, in rectangular and polar coordinates. The measured track is superimposed on the estimated track computed from the TLE
- the measured Elevation-Azimuth target track, in rectangular and polar coordinates.
- the graph of the Range errors relative to the input TLE. The error average and standard deviation is computed and presented on the graph
- the graph of the Doppler errors relative to the input TLE. The error average and standard deviation is computed and presented on the graph
- the and the target's SNR in dB.

Due to the crowded electromagnetic environment the radar operates in, composed of both reflections from the communication tower and a C-band radio link transmission, the user interface also contains a tool for removing the outliers produced by the interferences.

3. RADAR MEASUREMENT

3.1 Detection capability

Being a C-band radar, the Cheia radar is sensitive to weather. The high environmental humidity levels, either through fog, rain, snow, thick clouds or just winter with mild temperatures, introduce supplemental attenuation, thus reducing its detection capabilities.

The detection capability of the radar was tested in dry weather using the small RCS test satellite Calsphere 4A (Norad ID 1520), RCS= 0.0448m^2, Perigee= 1,081.3km, Apogee =1,182.2km [14]. The result of the test is presented in Figure 5.

The detection capability of the radar was also tested in bad weather using the large RCS test satellite EGS Ajisai (Norad ID 16908), RCS= 3.9811 m^2, Perigee= 1,485.9 km, Apogee = 1,503.5 km [14]. The result of the test is presented in Figure 6.

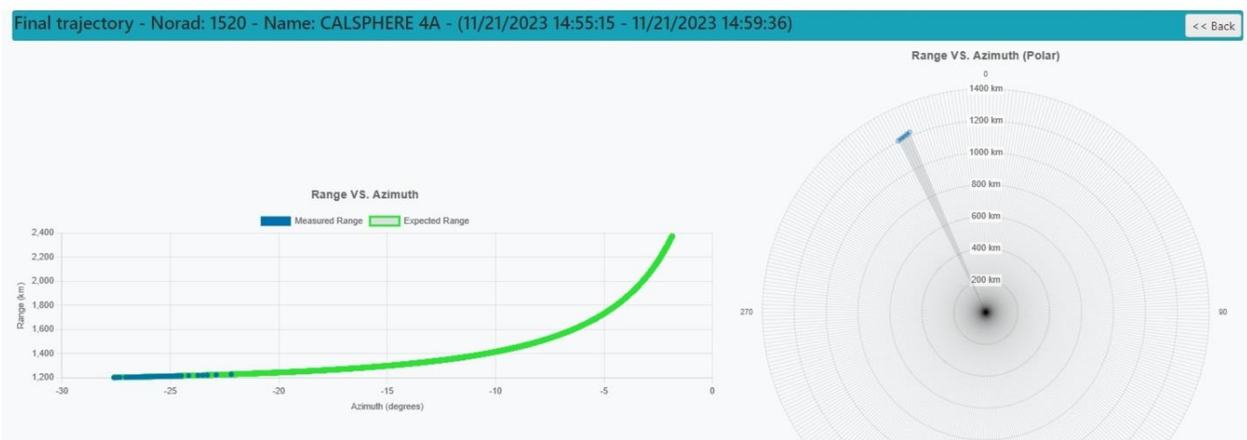

Figure 5 Detection range for Calsphere 4A

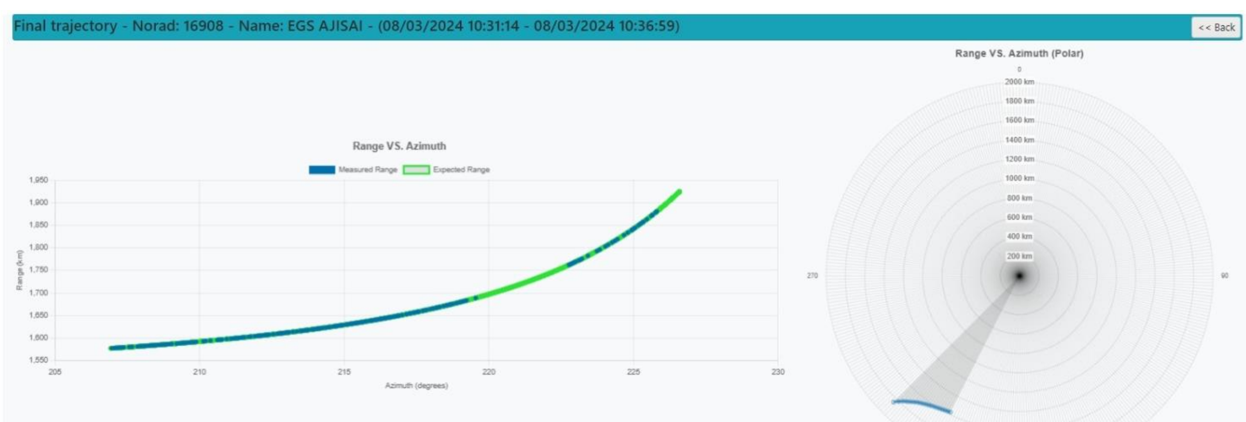

Figure 6 Detection range for EGS Ajisai

Both chosen test satellites have a spherical shape in order to eliminate the influence of the RCS directivity.

The minimum trackable target RCS at 1000 km, computed using the equation

$$RCS_{1000} = RCS_{meas}\left(\frac{1000}{R_{Max\ meas}}\right)^4$$

is presented in Table 2.

Table 2 Detection capability of the Cheia radar

Satellite	Parameter	Value
Calsphere 4A	Max Range (km)	1220
	Elevation Max Range	66.0
	SNR (dB)	12.92
	RCS_{1000} (m^2)	0.020
	RCS equivalent size (cm)	16
EGS Ajisai	Max Range (km)	1880
	Elevation Max Range	50.5
	SNR (dB)	13.86
	RCS_{1000} (m^2)	0.318
	RCS equivalent size (cm)	60

Table 2 shows that bad weather can reduce significantly the detection capability, by more than 10 dB.

3.2 Range and Doppler accuracy

The accuracy of the radar measurements was tested using the calibration satellite EGS-Ajisai by comparing the radar measured positions with the satellite precise positions (<1m accuracy) measured by optical means (SLRs) and published periodically by EDC [13].

Ajisai is a passive spherical satellite of 2.15 m diameter and a mass of 685.2 kg, carrying 318 mirrors and 120 laser retroreflector assemblies (1436 corner cube reflectors) for precise satellite laser ranging (SLR) measurements from ground-based laser ranging stations. It is especially destined for precision orbit determination and is generally used for geodesic purposes. It has a near-circular orbit with a perigee of approximately 1490 km, eccentricity 0.001, inclination 50°and period of 116 minutes.

The measured data are compared to the input TLE data and the to the precise data form the same epoch. The comparison is made for the Range, Doppler and angular data separately.

Figure 7 presents the Range and Doppler errors of the radar measurements in the visibility window starting at 28.07.2024 17:59:49 UTC, relative to the input data computed from the last available TLE. The range error is down slanted showing that there is a negative time delay between the TLE and the measurements. The spikes are outliers produced by the environmental interferences. As the radar distance to the satellite decreases, the spikes decrease since the received signal increases and becomes larger than the interferences.

Figure 8 presents the Range and Doppler errors of the radar measurements in the same visibility window (28.07.2024 17:59:49 UTC) relative to the post factum processed positioning data published by EDC [13].

Figure 9 presents the Range and Doppler errors of the radar measurements in the visibility window starting at 31.07.2024 13:14:19 UTC relative to the post factum processed positioning data (real trajectory)

Figure 10 presents the Range and Doppler errors of the radar measurements in the visibility window starting at 20.08.2024 11:25:18 UTC relative to the post factum processed positioning data (real trajectory), while Figure 11 presents the errors for the measurement in the visibility window starting at 21.08.2024 08:28:46 UTC. The figures show the Romanian local time (workstation time) and not the UTC time.

The averages and standard deviations for several measurements are presented in Table 3.

Table 3 Statistics for several measurements

Measurement no.	1	2	3	4	5	6	7
Range average (m)	11	-27	2	-23	-10	-20	1
Range std. dev. (m)	40	19	32	20	56	31	28
Doppler average (m/s)	0	0	0	0	0	0	0
Doppler std. dev. (m/s)	1	1	1	1	2	1	1
Measurements	384	699	844	620	370	818	255

Data in the table, takes account of all measured data, including the outliers. By removing the outliers, the dispersion can be significantly reduced. Measurements 1 and 5 are strongly affected by outliers produced by a radio link placed on the tower between the antennas.

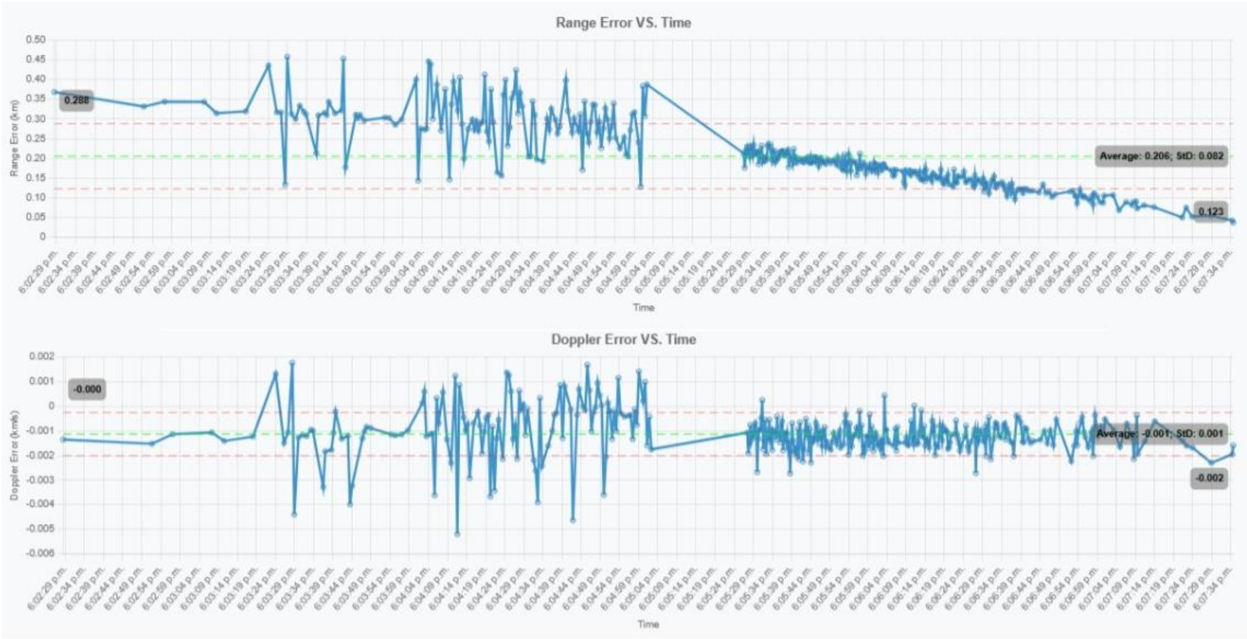

Figure 7 Range and Doppler errors for the measurement of Ajisai on 28.07.2024, window at 17:59:49 UTC (TLE reference)

Figure 8 Range and Doppler errors for Ajisai on 28.07.2024, window at 17:59:49 UTC (real trajectory reference)

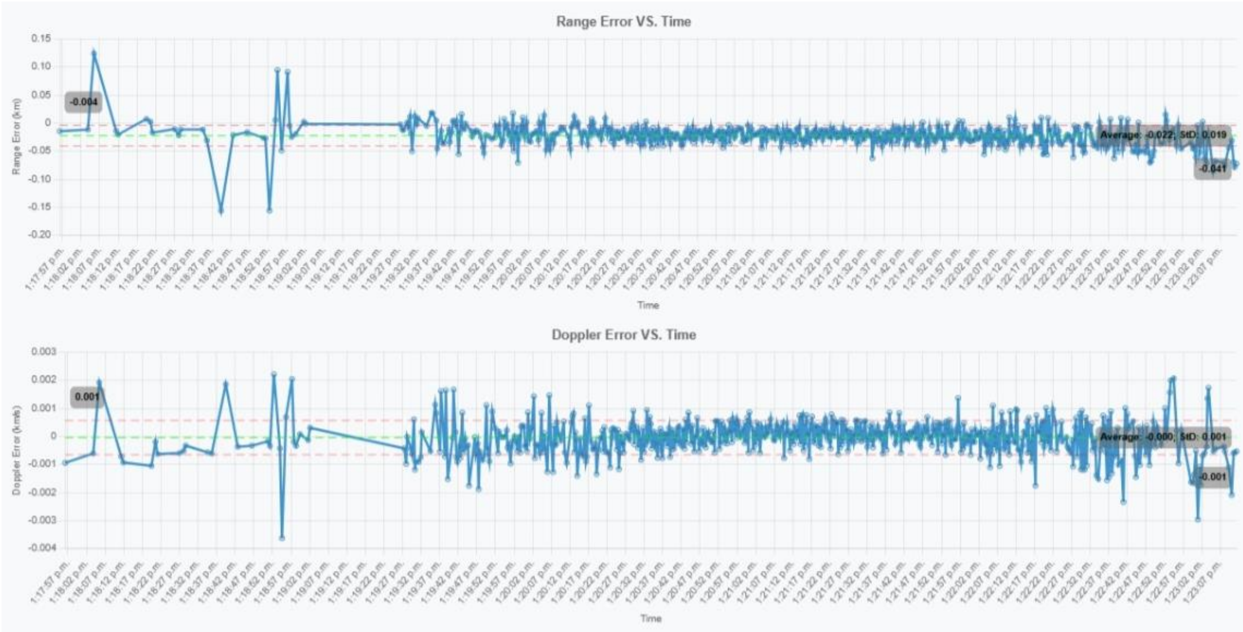

Figure 9 Range and Doppler errors for Ajisai on 31.07.2024, window at 13:14:19 UTC (real trajectory reference)

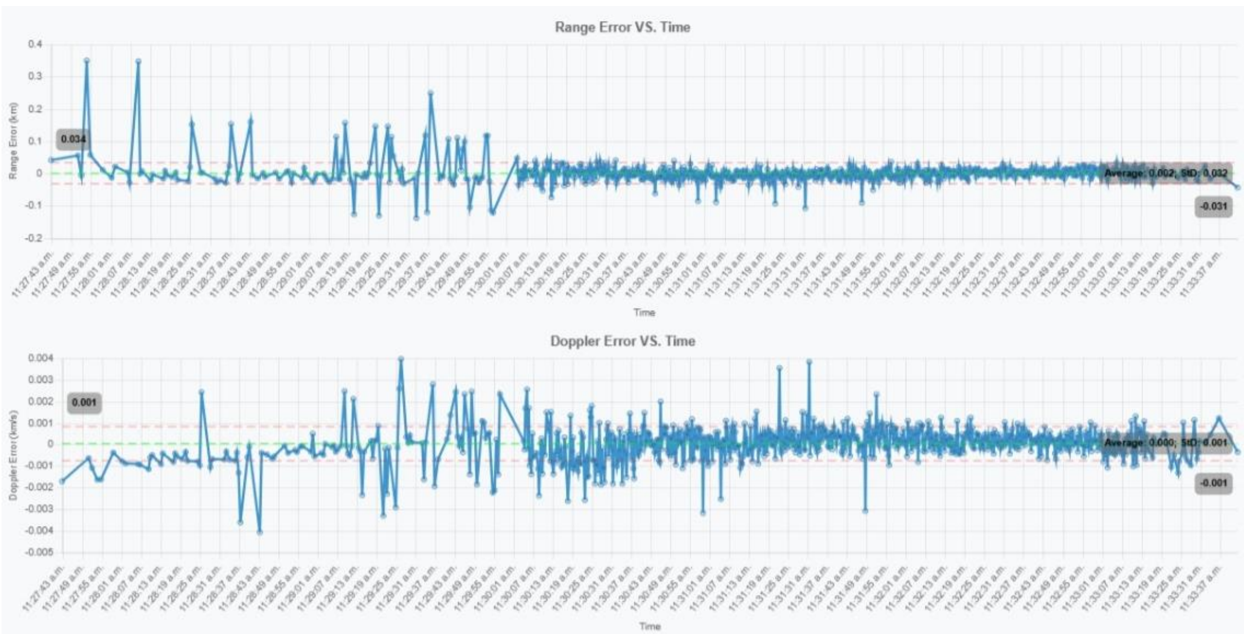

Figure 10 Range and Doppler errors for Ajisai on 20.08.2024, window at 11:25:18 UTC (real trajectory reference)

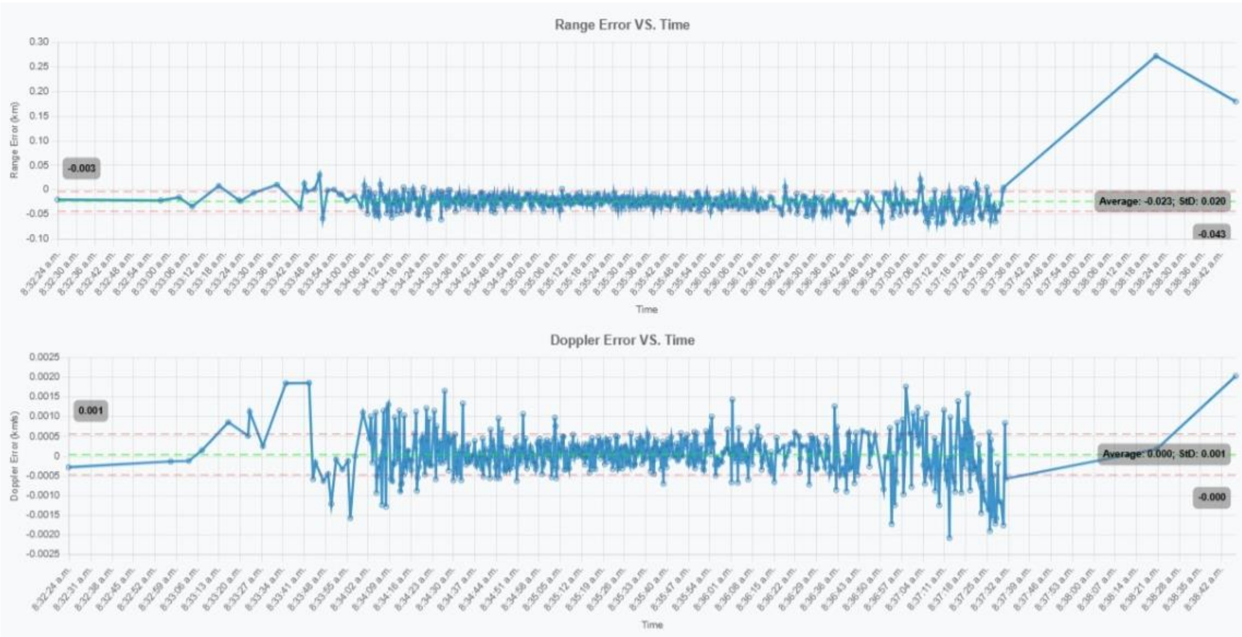

Figure 11 Range and Doppler errors for Ajisai on 21.08.2024, 08:28:46 UTC (real trajectory reference)

3.3 Angular accuracy

The azimuth and elevation errors of the measurements, that are really the TLE data confirmed by the radar, are precise enough for the radar tracking.

Figure 12 Azimuth and Elevation errors for Ajisai on 20.08.2024, 11:25:18 UTC (real trajectory reference) presents the Azimuth and Elevation errors for Ajisai on 20.08.2024, 11:25:18 UTC, while Figure 13 presents the same errors for Ajisai on 21.08.2024, 08:28:46 UTC. All errors are in mdeg and are computed relative to the real trajectories of the satellite.

The errors are below 55 mdeg which is the half power beamwidth of the antenna. The variation of the errors suggests that the antennas movement is not entirely smooth, due to their considerable age.

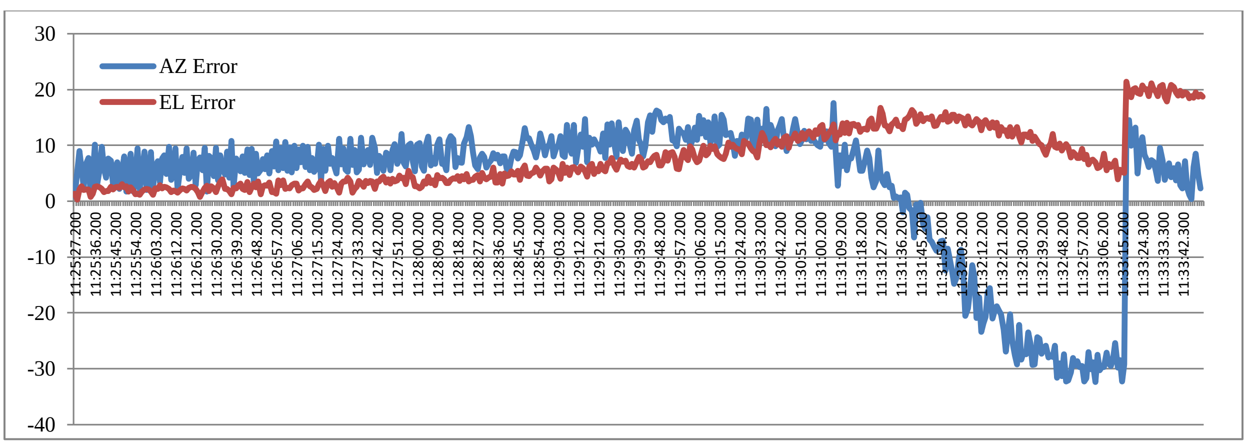

Figure 12 Azimuth and Elevation errors for Ajisai on 20.08.2024, 11:25:18 UTC (real trajectory reference)

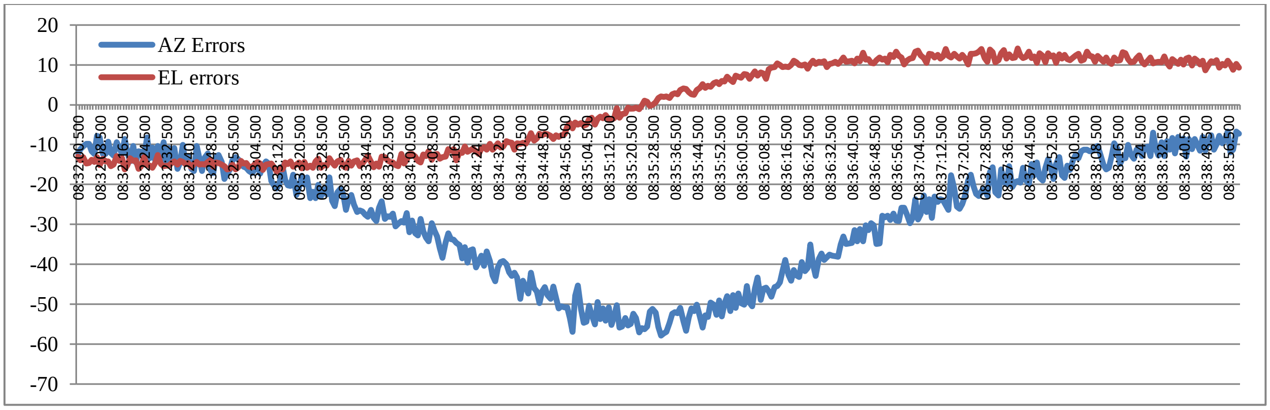

Figure 13 Azimuth and Elevation errors for Ajisai on 21.08.2024, 08:28:46 UTC (real trajectory reference)

4. EFFECT OF INTERFERENCES

The environmental perturbations, produced by the radio link operating on the pylon placed between the antennas and by the pylon itself (through reflections), do not prevent the operation of the radar but affect the measurements' precision. For this reason, a processing tool was provided in the user interface of the radar. The perturbations affect the measurements' precision in two ways: the reflections from the tower have an overall effect modifying the Range measurements average value and introducing outliers, while the radio link transmissions affect the measurements only partially, by strongly affecting the local average and the dispersion.

Figure 14 presents the effect of tower reflection on the measurement errors. The reflections affect mainly the range measurement because of the way the processing is performed into the radar.

Figure 15 presents the effect of the radio link transmission on the radar measurement errors. The transmissions affect both range and Doppler measurements but on limited time intervals.

Figure 14 Effect of reflections affecting range errors average and dispersion

Figure 15 Effect of radio link transmissions affecting range and Doppler errors average and dispersion

5. CONCLUSIONS, LESSONS LEARNED

It is possible to retrofit pairs of old satellite communication antennas into a space radar. However the retrofit process is more complicated than transforming an antenna for radio astronomy use. The retrofit requires mostly COTS or customized COTS but also some especially made components.

The retrofit can be performed without replacing the feeders of the antennas if the antenna initially designed bandwidth is used.

The antennas need not be in the same site but they need a dedicated, latency controlled, communication link.

The retrofit into a FMCW radar with exclusive frequency domain processing is particularly useful since most old communication antennas have relatively low transmitting power limit and a very good quality feeder. The frequency domain processing can take advantage of the low modulation frequency required by the very long ranges the radar scans.

Additionally, the FMCW radar operates adequately even in electromagnetically polluted environments which is an important advantage. However, the phase noise of interfering transmitters, will reduce its detection capability.

If very high accuracy is paramount, then special measures of removing obstacles from the antennas near field beam have to be observed. Additionally, electromagnetic environment control measures have to be applied.

It is possible to increase the radar detection capability without increasing the transmitted power, by improving the antennas electromagnetic separation.

The radar can be designed with autotracking capability but this cannot be used if high interference, either as reflections or as transmissions, is present. If both antennas are not mechanically identical, the autotrack error signal should be applied only to the receiving antenna

If the radar C-band is used, weather (humidity) dependency should be expected. In the case of polluted electromagnetic environment, the bad weather has a dual effect. It attenuates the radar probing signal and enhances the effect of the interferences since they are close range and thus not significantly attenuated.

To accurately measure a space object, the use of a dedicated high accuracy time-stamping device is compulsory.

6. REFERENCES

[1] EU Space Programme 2021–2027. https://www.consilium.europa.eu/en/policies/eu-space-programme/ (accessed on 20 January 2024).

[2] ESA'S Annual Space Environment Report 2021. https://www.esa.int/Safety_Security/Space_Debris/ESA_s_Space_Environment_Report_2021 (accessed on 22 January 2023).

[3] European Parliament and Council of the European Union. Decision No 541/2014/EU of the European Parliament and of the Council of 16 April 2014 establishing a Framework for Space Surveillance and Tracking Support. *Off. J. Eur. Union* **2014**, *57*, 227–236. https://eur-lex.europa.eu/legal-content/EN/TXT/?uri=CELEX%3A02014D0541-20180802

[4] Donald R. Wehner, "High-Resolution Radar", Artech House Radar Library

[5] Bassem R. Mahafza, Ph.D., "Radar Systems Analysis and Design using MATLAB", Chapman & Hall/Crc, Boca Raton London New York Washington, D.C.

[6] Barton, D. K., *Modern Radar System Analysis*, Artech House, Norwood, MA, 1988.

[7] Bira, C.; Rusu-Casandra A., A. Dataset of Spatial Objects Acquired Using Romania's First Ground-Based Space Tracking Radar. In Proceedings of the 14th International Conference on Communications COMM 2022, Bucharest, Romania, 16–18 June 2022.

[8] Ionescu L., Rusu-Casandra A., Bira C., Tatomirescu A., Tramandan I., Scagnoli R., Istriteanu D., Popa A.E., Development of the Romanian Radar Sensor for Space Surveillance and Tracking Activities. Sensors 2022, 22(9), 3546; 19 p, https://doi.org/10.3390/s22093546, ISSN: 1424-8220

[9] Tatomirescu, A.; Rusu-Casandra A., C-Band FMCW RADAR Receiver Architecture for Space Debris Observation. In Proceedings of the 14th International Conference on Communications COMM 2022, Bucharest, Romania, 16–18 June 2022.

[10] Tramandan, I; Rusu-Casandra A., Real-Time Monitoring and Command System for the Cheia Space Surveillance and Tracking Radar. In Proceedings of the ISETC 2022 Conference, Timisoara, Romania, November 2022.

[11] Societatea Naţională de Radiocomunicaţii S.A. (RADIOCOM), Centrul de Comunicaţii Prin Satelit CHEIA. https://www.radiocom.ro/Materiale/Cheia/Centrul%20de%20Comunicatii%20prin%20Satelit%20CHEIA.pdf (accessed on 2 February 2021).

[12] Ionescu L., Scagnoli R., Istriteanu D., Turcu V: "*Cheia antennas retrofit to a space tracking radar"* 1st NEO and Debris Detection Conference, 22-24 January 2019, Darmstadt, Germany, published by ESA Space Safety Programme Office (https://conference.sdo.esoc.esa.int/proceedings/list?search=&conference=2&publishing-year=2&title=&author-name=&author-organisation=&abstract-full-text=&field_keywords_value=Cheia)

[13] EUROLAS Data Center (EDC) Deutsches Geodätisches Forschungsinstitut Technische Universität München, https://edc.dgfi.tum.de/pub/slr/products/orbits/ajisai/.

[14] N2YO.COM site, n2yo.com